Journal of Naval Architecture and Marine Engineering
December, 2011
DOI: 10.3329/jname.v8i2.5055 http://www.banglajol.info

VISCOUS DISSIPATION AND JOULE HEATING EFFECTS ON STEADY MHD COMBINED HEAT AND MASS TRANSFER FLOW THROUGH A POROUS MEDIUM IN A ROTATING SYSTEM

Md. Mahmud Alam[1], M. Delowar Hossain[2] and M. Arif Hossain[2]

[1]Mathematics Discipline, Science Engineering & Technology School, Khulna University, Khulna-9208, Bangladesh, Email: alam_mahmud2000@yahoo.com

[2]Department of Mathematics, Khulna University of Engineering & Technology, Khulna-9203, Bangladesh

Abstract:

Viscous dissipation and Joule heating effects on steady MHD combined heat and mass transfer flow through a porous medium along a semi-infinite vertical porous plate in a rotating system has been studied numerically. The boundary layer equations have been transformed into dimensionless coupled nonlinear ordinary differential equations by using appropriate transformations. The similarity solutions of the transformed dimensionless equations for the flow field and heat and mass transfer characteristics are obtained by shooting iteration technique. Numerical results are presented in the form of primary and secondary velocities, temperature and concentration distributions for different parameters entering into the analysis. Finally, the effects of the pertinent parameters on the Skin-friction coefficients, Nusselt number and Sherwood number are also examined.

***Keywords**:* MHD, Joule heating, porous medium, rotating system.

1. Introduction

In a rotating system, the Coriolis force is very significant as compared to viscous and inertia forces occurring in the basic fluid equations. In Stellar studies it is generally admitted that the Coriolis force due to Earth's rotation has a strong effect on the hydromagnetic flow in the Earth's liquid core. Considering this aspect of the rotational flows, model studies were carried out on MHD free convection and mass transfer flows in a rotating system by many investigators of whom the names Debnath(1975), Debnath et al.(1979), Raptis and Perdikis(1982) are worth mentioning.

In the above-mentioned work, the Soret and Dufour effects were neglected on the basis that they are of a smaller order of magnitude than the effects described by Fourier's and Fick's laws. The thermal diffusion (Soret) effect, for instance, has been utilized for isotope separation and in mixture between gases with very light molecular weight (H_2, H_e) and of medium molecular weight (N_2, air), the diffusion-thermo (Dufour) effect was found to be of order of considerable magnitude such that it cannot be ignored (Eckert and Drake, 1972). In view of the importance of above-mentioned effects, Kafoussias and Williams (1995) studied Soret and Dufour effects on mixed free-forced convection and mass transfer boundary layer flow with temperature dependent viscosity. Anghel et al.(2000) investigated the Dufour and Soret effects on free-convection boundary layer flow over a vertical surface embedded in a porous medium. Recently, Postelnicu (2004) studied numerically the influence of a magnetic field on heat and mass transfer by natural convection from vertical porous plate in porous media considering Soret and Dufour effects. Quite recently, Alam and Rahman (2006) investigated the Dufour and Soret effects on mixed convection flow past a vertical porous flat plate with variable suction.

Hence, our objective is to investigate the steady MHD combined heat and mass transfer flow through a porous medium past an infinite vertical porous plate with viscous dissipation and Joule heating effects in a rotating system. The effect of Joule heating on MHD combined heat and mass transfer flow of an electrically conducting viscous incompressible fluid past an infinite plate was, however considered by Hossain (1990). The governing

1813-8235 (Print), 2070-8998 (Online) Received on: May 2010

equations of the problem contain the partial differential equations, which are transformed by similarity transformation into dimensionless ordinary coupled non-linear differential equations. The obtained equations are solved numerically by sixth order Runge-Kutta method along with the Nachtsheim-Swigert iteration technique. The obtained solutions are shown graphically as well as in tabular form.

2. The Governing Equations

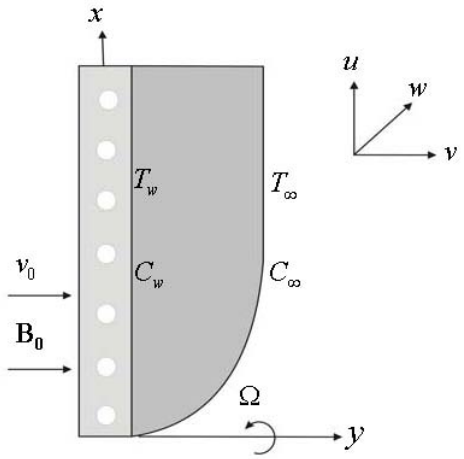

Figure 1: Physical configuration and coordinate system.

Let us consider a steady MHD combined heat and mass transfer flow of an electrically conducting viscous fluid through a porous medium along semi-infinite vertical porous plate $y = 0$ in a rotating system. The flow is also assumed to be moving with a uniform velocity U_o, which in the x-direction is taken along the plate in the upward direction and *y*-axis is normal to it. Initially the plate is at rest, after that the whole system is allowed to rotate with a constant angular velocity Ω about the y-axis. The temperature and the species concentration at the plate are constantly raised from T_w and C_w to T_∞ and C_∞ respectively, where T_∞ and C_∞ are the temperature and species concentration of the uniform flow respectively.

A uniform magnetic field B is taken to be acting along the *y*-axis which is assumed to be electrically non-conducting. We assumed following (Pai, 1962) that the magnetic Reynolds number of the flow is taken to be small enough so that the induced magnetic field is negligible in comparison with applied one, so that $\mathbf{B} = (0, B_0, 0)$ and the magnetic lines of force are fixed relative to the fluid. The equation of conservation of charge $\nabla.\mathbf{J} = 0$ gives $J_y = \text{constant}$, where the current density $\mathbf{J} = (J_{x,} J_{y,} J_z)$. Since the plate is electrically non-conducting, this constant is zero and hence $J_y = 0$ at the plate and also zero everywhere. The physical configuration considered here is shown in Figure. 1. It is assumed that the plate is semi-infinite in extent and hence all the physical quantities depend on y and x. Thus accordance with the above assumptions and Boussinesq's approximation, the basic equations relevant to the problem is;

$$\frac{\partial u}{\partial x} + \frac{\partial v}{\partial y} = 0 \tag{1}$$

$$u\frac{\partial u}{\partial x} + v\frac{\partial u}{\partial y} = \upsilon\frac{\partial^2 u}{\partial y^2} + g\beta\left(T - T_\infty\right) + g\beta^*\left(C - C_\infty\right) + 2\Omega w + \frac{\upsilon}{K'}\left(U_0 - u\right) + \frac{\sigma' B_0^{\,2}}{\rho}\left(U_0 - u\right) \tag{2}$$

$$u\frac{\partial w}{\partial x} + v\frac{\partial w}{\partial y} = \upsilon\frac{\partial^2 w}{\partial y^2} + 2\Omega\left(U_0 - u\right) - \frac{\upsilon}{K'}w - \frac{\sigma' B_0^{\,2} w}{\rho} \tag{3}$$

$$u\frac{\partial T}{\partial x}+v\frac{\partial T}{\partial y}=\frac{k}{\rho c_p}\frac{\partial^2 T}{\partial y^2}+\frac{D_m k_T}{c_s c_p}\frac{\partial^2 C}{\partial y^2}+\frac{\upsilon}{c_p}\left[\left(\frac{\partial u}{\partial y}\right)^2+\left(\frac{\partial w}{\partial y}\right)^2\right]+\frac{\sigma' B_0^2}{\rho c_p}\left[(U_0-u)^2+w^2\right] \tag{4}$$

$$u\frac{\partial C}{\partial x}+v\frac{\partial C}{\partial y}=D_m\frac{\partial^2 C}{\partial y^2}+\frac{D_m k_T}{T_m}\frac{\partial^2 T}{\partial y^2} \tag{5}$$

The boundary conditions for the problem are;

$$\left.\begin{aligned} &u=0, v=v_0(x),\ w=0, T=T_w,\ C=C_w \quad at\ y=0\\ &u=U_0, \qquad\qquad w=0, T\to T_\infty, C\to C_\infty\ as\ y\to\infty \end{aligned}\right\} \tag{6}$$

Following the work of Sattar (1993), a transformation is now made as,

$u_1=U_0-u, \quad \therefore u=U_0-u_1$

Equations (1) – (5) and the boundary conditions (6), respectively, transform to;

$$-\frac{\partial u_1}{\partial x}+\frac{\partial v}{\partial y}=0 \tag{7}$$

$$(U_0-u_1)\frac{\partial u_1}{\partial x}+v\frac{\partial u_1}{\partial y}=\upsilon\frac{\partial^2 u_1}{\partial y^2}-g\beta(T-T_\infty)\ -g\beta^*(C-C_\infty)-2\Omega w-\frac{\upsilon}{K'}u_1-\frac{\sigma' B_0{}^2}{\rho}u_1 \tag{8}$$

$$(U_0-u_1)\frac{\partial w}{\partial x}+v\frac{\partial w}{\partial y}=\upsilon\frac{\partial^2 w}{\partial y^2}+2\Omega u_1-\frac{\upsilon}{K'}w-\frac{\sigma' B_0{}^2 w}{\rho} \tag{9}$$

$$(U_0-u_1)\frac{\partial T}{\partial x}+v\frac{\partial T}{\partial y}=\frac{k}{\rho c_p}\frac{\partial^2 T}{\partial y^2}+\frac{D_m k_T}{c_s c_p}\frac{\partial^2 C}{\partial y^2}+\frac{\upsilon}{c_p}\left[\left(\frac{\partial u_1}{\partial y}\right)^2+\left(\frac{\partial w}{\partial y}\right)^2\right]+\frac{\sigma' B_0^2}{\rho c_p}\left[u_1^2+w^2\right] \tag{10}$$

$$(U_0-u_1)\frac{\partial C}{\partial x}+v\frac{\partial C}{\partial y}=D_m\frac{\partial^2 C}{\partial y^2}+\frac{D_m k_T}{T_m}\frac{\partial^2 T}{\partial y^2} \tag{11}$$

$$\left.\begin{aligned} &u_1=U_0, v=v_0(x), w=0, T=T_w, C=C_w \quad at\ \ y=0\\ &u_1=0, \qquad\qquad w=0, T\to T_\infty, C\to C_\infty\ \ as\ \ y\to\infty \end{aligned}\right\} \tag{12}$$

where u, v, w are the velocity components in the x, y, z direction respectively, υ is the kinematics viscosity, g is the acceleration due to gravity, ρ is the density, β is the coefficient of volumetric thermal expansion, β^* is the volumetric mass expansion. T, T_w and T_∞ are the temperature of the fluid inside the thermal boundary layer, the plate temperature and the fluid temperature in the free stream, respectively, while C, C_w, C_∞ are the corresponding concentrations. Also K' is the permeability of the porous medium, κ is the thermal conductivity of the medium, D_m is the coefficient of mass diffusivity, c_p is the specific heat at constant pressure, T_m is the mean fluid temperature, k_T is the thermal diffusion ratio, c_s is the concentration susceptibility and other symbols have their usual meaning.

3. Mathematical Formulations

In order to solve Equations (8)-(11) under the boundary conditions (12), we adopt the well-defined similarity analysis to attain similarity solutions.

For this purpose, the following similarity transformations are now introduced;

$$\eta=y\sqrt{\frac{U_0}{2\upsilon x}} \tag{13}$$

$$g_0(\eta)=\frac{w}{U_0} \tag{14}$$

$$\theta(\eta)=\frac{T-T_\infty}{T_w-T_\infty} \tag{15}$$

$$\phi(\eta)=\frac{C-C_\infty}{\bar{x}(C_0-C_\infty)} \tag{16}$$

$$\psi=\sqrt{2\upsilon x U_0}\,f(\eta) \tag{17}$$

$$u_1=\frac{\partial\psi}{\partial y}=U_0 f'(\eta) \tag{18}$$

$$\therefore \frac{u}{U_0}=1-f'(\eta)$$

Now for reasons of similarity, the plate of concentration is assumed to be

$$C_w(x)=C_\infty+\bar{x}(C_0-C_\infty), \tag{19}$$

where C_0 is considered to be mean concentration and $\bar{x}=\frac{xU_0}{\upsilon}$.

The continuity equation (7) then yields

$$v=\frac{\partial\psi}{\partial x}=-\sqrt{\frac{\upsilon U_0}{2x}}\;\left[\eta f'(\eta)-f(\eta)\right]\quad . \tag{20}$$

Also we have, $f_w=v_0(x)\sqrt{\frac{2x}{U_o\upsilon}}$ (21)

Where f_w is the suction parameter or transpiration parameter and clearly in (21) $f_w<0$ corresponds to suction and $f_w>0$ corresponds to injection at the plate.

From equations (8) - (12) and (13)-(21), we have the following dimensionless ordinary coupled non-linear differential equations

$$f'''+(\eta-1)f''-G_r\theta-G_m\phi-Rg_0-(K+M)f'=0 \tag{22}$$

$$g_0''+(\eta-f)g_0'+Rf'-(K+M)g_0=0 \tag{23}$$

$$\theta''+P_r(\eta-f)\theta'+D_f\phi''+P_rE_c\left\{(f'')^2+(g_0')^2\right\}+P_rE_cM\left\{(f')^2+(g_0)^2\right\}=0 \tag{24}$$

$$\phi''+S_c(\eta-f)\phi'+2S_c(f'-1)\phi+S_0\theta''=0 \tag{25}$$

with the corresponding boundary conditions

$$\left.\begin{array}{l} f=f_w,\ f'=1,\ g_0=0,\ \theta=1,\ \phi=1 \quad \text{at}\ \ \eta=0 \\ f'=0,\qquad\quad g_0=0,\ \theta=0,\ \phi=0 \quad \text{as}\ \ \eta\to\infty \end{array}\right\} \tag{26}$$

where $G_r=\frac{g\beta(T_w-T_\infty)2x^3}{\upsilon^2}$ is the Grashof number, $G_m=\frac{g\beta^*(C_w-C_\infty)2x^3}{\upsilon^2}$ the modified Grashof number, $K=\frac{2\upsilon x}{K'U_0}$ the Permeability parameter, $M=\frac{2x\sigma' B_0^{\,2}}{\rho U_0}$ the Magnetic parameter and $R=\frac{4\Omega x}{U_0}$ the rotational parameter, $P_r=\frac{\rho\upsilon c_p}{\kappa}$ the Prandtl number, $D_f=\frac{D_m k_T\rho}{c_s K'}\frac{(C_w-C_\infty)}{(T_w-T_\infty)}$ the Dafour number, $E_c=\frac{U_0^{\,2}}{c_p(T_w-T_\infty)}$ the Eckert number, $S_c=\frac{\upsilon}{D_m}$ the Schmidt number and $S_0=\frac{k_T}{T_m}\frac{(T_w-T_\infty)}{(C_w-C_\infty)}$ the Soret number.

3.1 Skin-friction coefficients, Nusselt number and Sherwood number

The quantities of chief physical interest are the skin friction coefficients, the Nusselt number and the Sherwood number. The wall skin frictions are denoted by

$\tau_x = \mu\left(\frac{\partial u}{\partial y}\right)_{y=0}$ and $\tau_z = \mu\left(\frac{\partial w}{\partial y}\right)_{y=0}$ which are proportional to $\left(\frac{\partial^2 f}{\partial \eta^2}\right)_{\eta=0}$ and $\left(\frac{\partial g_0}{\partial \eta}\right)_{y=0}$.

The Nusselt number is denoted by $N_u = -\frac{1}{\Delta T}\left(\frac{\partial T}{\partial y}\right)_{y=0}$ which is proportional to $\left(\frac{\partial \theta}{\partial \eta}\right)_{\eta=0}$.

The Sherwood number is denoted by $S_h = -\frac{1}{\Delta C}\left(\frac{\partial C}{\partial y}\right)_{y=0}$ which is proportional to $\left(\frac{\partial \phi}{\partial \eta}\right)_{\eta=0}$.

The numerical values of the skin-friction coefficients, the Nusselt number and the Sherwood number are sorted in Tables 1-5.

4. Calculation Procedure And Numerical Technique

4.1. Calculation procedure

Alam et. al (2006) has used shooting method to solve their problem. The same solution technique has been used to solve our problem and the details solution procedures are given below. The system of non-linear ordinary differential equations (22)-(25) together with the boundary conditions (26) are similar and solved numerically using Nachtsheim-Swigert shooting iteration technique (guess the missing value) along with sixth order Runge-Kutta initial value solver.

In a shooting method, the missing (unspecified) initial condition at the initial point of the interval is assumed, and the differential equation is then integrated numerically as an initial problem to the terminal point. The accuracy of the assumed missing initial condition is then checked by comparing the calculated value of the dependent variable at the terminal point with its given value there. If a difference exists, another value of the missing initial condition must be assumed and the process is repeated. This process is continued until the agreement between the calculated and the given condition at the terminal point is within the specified degree of accuracy. For this type of iterative approach, one naturally inquires whether or not there is a symmetric way of finding each succeeding (assumed) value of the initial condition.

The method of numerically integrating a two-point asymptotic boundary value problem of the boundary-layer type, the initial value method is similar to an initial value problem. Thus it is necessary to estimate as many boundary conditions at the surface as were given at infinity. The governing differential equations are then integrated with these assumed surface boundary conditions. If the required outer boundary condition is satisfied, a solution has been achieved. However, this is not generally the case. Hence, a method must be devised to estimate logically the new surface boundary conditions for the next trial integration. Asymptotic boundary value problems such as those governing the boundary-layer equations are further complicated by the fact that the outer boundary condition is specified at infinity. In the trial integration infinity is numerically approximated by some large value of the independent variable. There is no a priorigenera method of estimating these values. Selecting too small maximum value for the independent variable may not allow the solution to asymptotically converge to the required accuracy.

Nachtsheim-Swigert developed an iteration method to overcome these difficulties. An extension of Nachtsheim-Swigert iteration scheme to the system of equations (22)-(25) and the boundary conditions (26) is straight forward. In equation (26) there are four asymptotic boundary conditions and hence four unknown surface conditions $f''(0)$, $g_0'(0)$, $\theta'(0)$ and $\phi'(0)$.

4.2. Numerical technique in brief

Within the context of the initial-value method and Nachtsheim-Swigert iteration technique the outer boundary conditions may be functionally represented as

$$\Phi_j(\eta_{max}) = \Phi_j\left(f''(0), g_0'(0), \theta'(0), \phi'(0)\right) = \delta_j,\ j = 1, 2, ...8, \tag{27}$$

Where $\Phi_1 = f', \Phi_2 = g_0, \Phi_3 = \theta, \Phi_4 = \phi, \Phi_5 = f'', \Phi_6 = g_0', \Phi_7 = \theta', \Phi_8 = \phi'$ and $\Phi_5, \Phi_6, \Phi_7, \Phi_8$ represent asymptotic convergence criteria.

Choosing $f''(0) = g_1, g_0'(0) = g_2, \theta'(0) = g_3, \phi'(0) = g_4$ and expanding in a first order Taylor's series after using equation (27) yields;

$$\Phi_j(\eta_{\max}) = \Phi_{j,C}(\eta_{\max}) + \sum_{i=1}^{4} \frac{\partial \Phi_j}{\partial g_i} \Delta g_i = \delta_j,\ \ j = 1, 2, ...8, \tag{28}$$

Where subscript 'C' indicates the value of the function at $\eta_{\max}$ determined from the trial integration.
Solution of these equations in a least-square sense require to determining the minimum value of

$$E = \sum_{j=1}^{8} \delta_j^2 \tag{29}$$

with respect to $g_i\,(i = 1, 2, 3, 4)$.

Now differentiating *E* with respect to g_i we obtain

$$\sum_{j=1}^{8} \delta_j \frac{\partial \delta_j}{\partial g_i} = 0 \tag{30}$$

Substituting Equation (28) into (30) after some algebraic calculation we obtain

$$\sum_{k=1}^{4} a_{ik} \Delta g_k = b_i,\ i = 1, 2, 3, 4, \tag{31}$$

where

$$a_{ik} = \sum_{j=1}^{8} \frac{\partial \Phi_j}{\partial g_i} . \frac{\partial \Phi_j}{\partial g_k},\ b_i = -\sum_{j=1}^{8} \Phi_{j,C} \frac{\partial \Phi_j}{\partial g_i},\ \ i, k = 1, 2, 3, 4, \tag{32}$$

Now solving the system of linear equations (31) using Cramer's rule we obtain the missing (unspecified) values of g_i as

$$g_i \equiv g_i + \Delta g_i \tag{33}$$

Thus adopting the numerical technique aforementioned, the solution of the non-linear ordinary differential equations (22)-(25) with the boundary conditions (26) are obtained together with sixth order Runge-Kutta initial value solver and determine the velocities, temperature and concentration as a function of the coordinate η.

4. Results and Discussion

In this paper, the effects of viscous dissipation and joule heating on steady MHD combined heat and mass transfer flow through a porous medium in a rotating system have been investigated using Nachtsheim-Swigerts shooting iteration technique. To study the physical situation of this problem, we have computed the numerical value of the velocities, temperature, concentration, within the boundary layer and also find the skin friction coefficients, Nusselt and Sherwood number at the plate. It can be seen that the solutions are affected by the parameters, namely suction parameter f_w, Grashof number G_r, modified Grashof number G_m, Permeability parameter K, Magnetic parameter M, Prandtl number P_r, Eckert number E_c, Dufour number D_f, Schmidt number S_c, Soret number S_o, Rotation parameter R.

The values of G_r, G_m are taken to be large, since these values corresponds to a cooling problem, i.e. Generally encountered in nuclear engineering in connection with the cooling of reactors. The result of numerical

calculations are presented in the form of primary (f') and secondary (g_0) velocities in Figures. (2)-(19) for different values of f_w , M , R, S_o , D_f , E_c, P_r, S_c, K. The values $0.2, 0.5, 0.71, 1, 2, 5$ are considered for Prandtl number P_r ($0.2, 0.5, 0.71$ for air and $1.0, 2.0, 5.0$ for water). The values $0.1, 0.5, 0.6, 0.95, 5, 10$ are also considered for Schmidt number S_c, which represent specific conditions of the flow (0.95 for CO_2 and $0.1, 0.5, 0.6, 5, 10$ for water). The values of other parameters are chosen arbitrarily. The effects of various parameters on secondary velocity are shown in Figures. 2-10. From Figure. 2, it can be seen that the primary velocity increases with the increase of suction parameter f_w, for both $f_w > 0$ and $f_w < 0$, indicating the usual fact that suction stabilizes the boundary layer growth. The free convection effect is also apparent in this figure. For $\eta = 1.5$, the velocity field is found to increase and reaches a maximum value in a region close to the leading edge of the plate, then gradually decreases to one. Figure. 3, shows the primary velocity for different values of magnetic parameter M and has a decreasing effect with increase of M. The magnetic field can therefore be used to control the flow characteristics. The variation of the primary velocity for different values of rotation parameter R is shown in Figure. 4. It is seen that the rotation parameter R has a minor decreasing effect on the primary velocity.

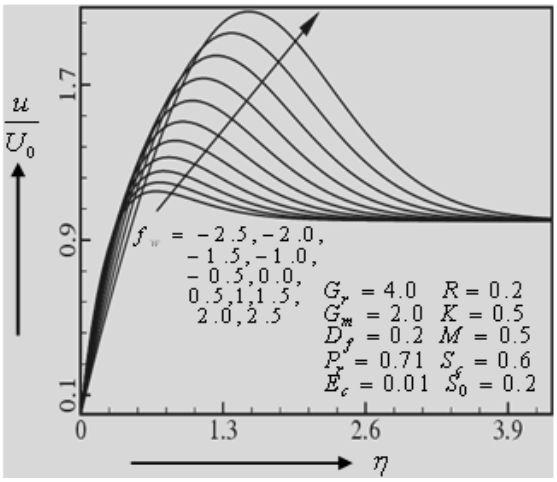

Figure 2: Primary velocity profiles for different values of f_w

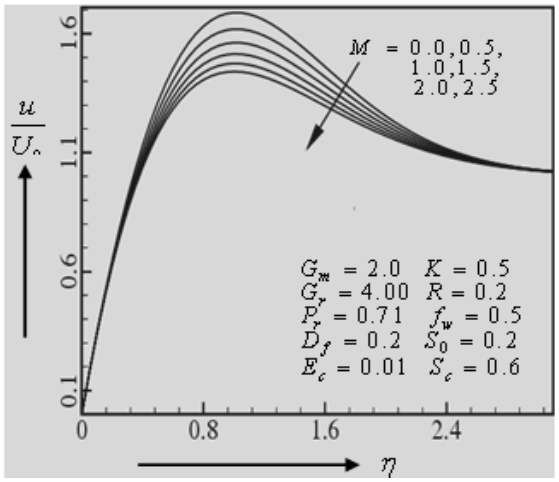

Figure 3: Primary velocity profiles for different values of M

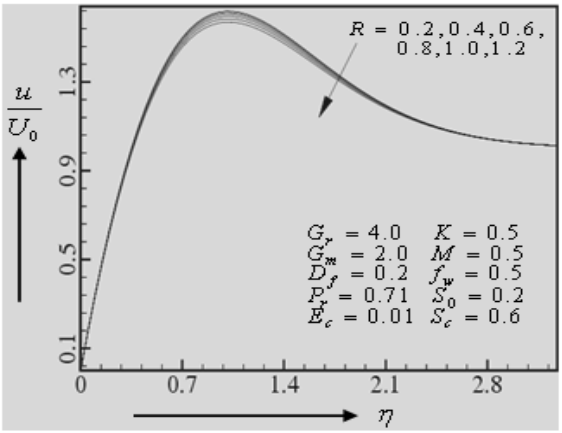

Figure 4: Primary velocity profiles for different values of R

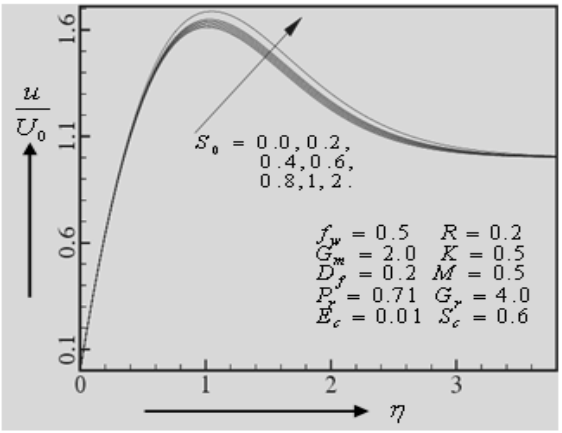

Figure 5: Primary velocity profiles for different values of S_0

In Figures 5-7 the variations of the primary velocity for different values of Soret number S_o, Dufour number D_f and the Eckert number E_c, are shown respectively. From these figures it is observed that the primary velocity uniformly increases with the increase of Soret number S_o, Dufour number D_f and the Eckert number E_c. In Figs. 8-10, the variations of the primary velocities for different values of Prandtl number P_r, Schmidt number S_c and permeability parameter K are shown respectively. Figures 8 and 9 show that the magnitude of the primary velocities have a overshoot behavior for small Prandtl number P_r and Schimdt number S_c. But for larger values of $P_r\,(P_r = 0.5)$ and S_c the velocities are found to decrease monotonically and hence there appears a thin boundary layer indicating the decrease of the free convection. Also the primary velocity decreases with the increase of permeability parameter K.

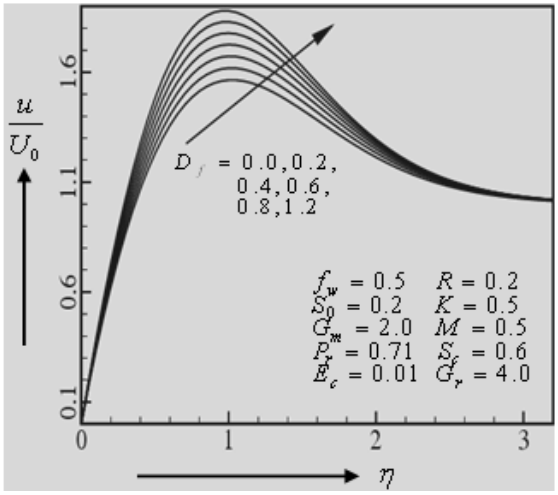

Figure 6: Primary velocity profiles for different values of D_f

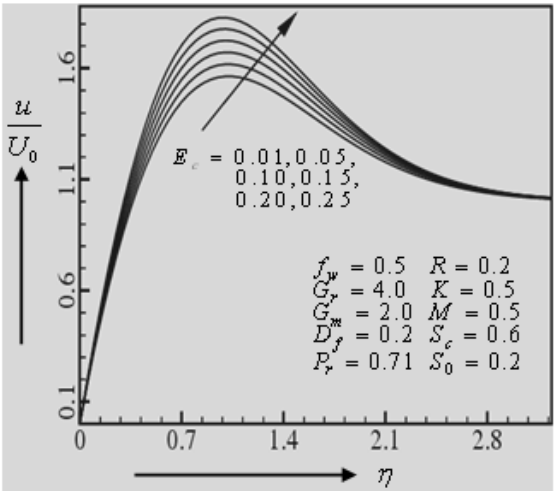

Figure 7: Primary velocity profiles for different values of E_c

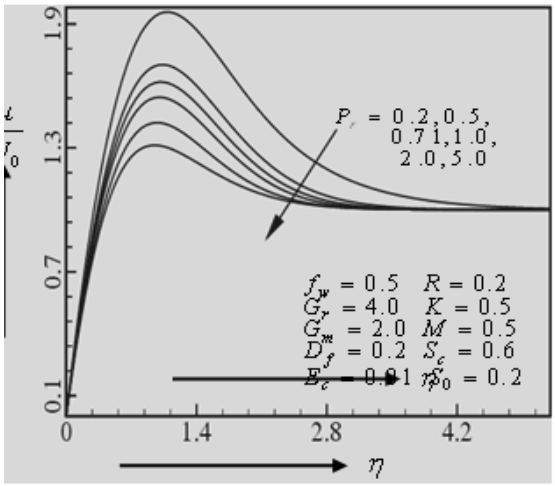

Figure 8: Primary velocity profiles for different values of P_r

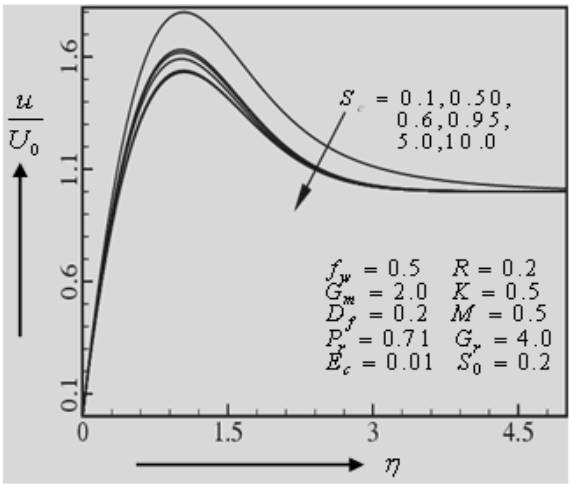

Figure 9: Primary velocity profiles for different values of S_c

The effects of various parameters on the secondary velocity are shown in Figs. 11-19. From Fugure 11, it can be seen that the secondary velocity field decreases with the increase of suction parameter f_w, for both $f_w > 0$

and $f_w < 0$, indicating the usual fact that suction stabilizes the boundary layer growth. The free convection effect is also apparent in this figure, for $\eta = 1.8$, the velocity field is found to decrease and reaches a minimum value in a region close to the lading edge of the plate, then gradually increase to zero. Figure. 12 shows the secondary velocity for different values of magnetic parameter M and shows a large increasing effect with increase of M.

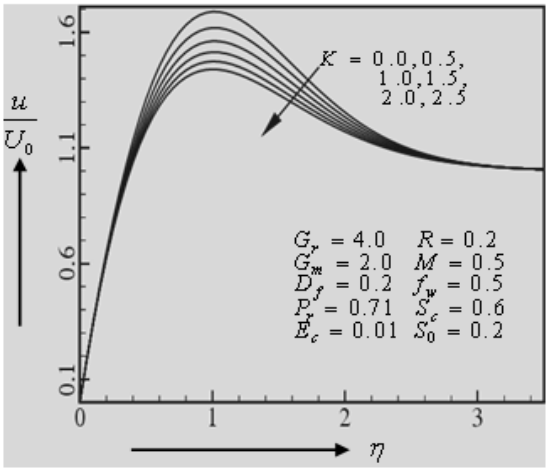

Figure 10: Primary velocity profiles for different values of *K*

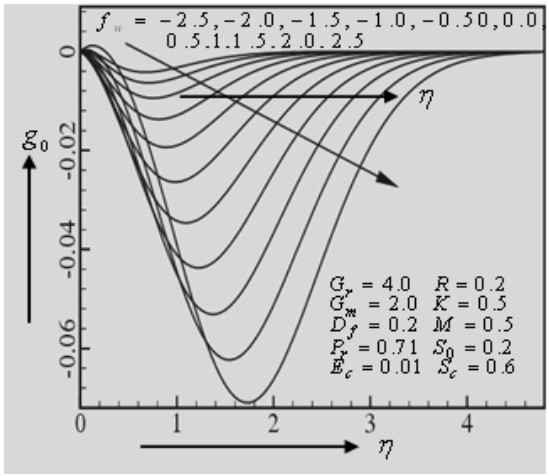

Figure 11: Secondary velocity profiles for different values of f_w

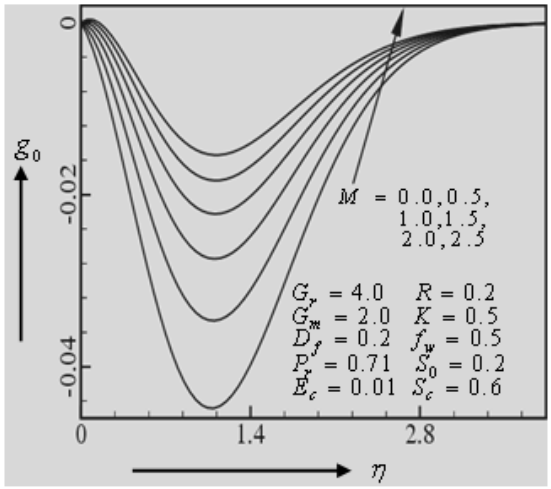

Figure 12: Secondary velocity profiles for different values of *M*

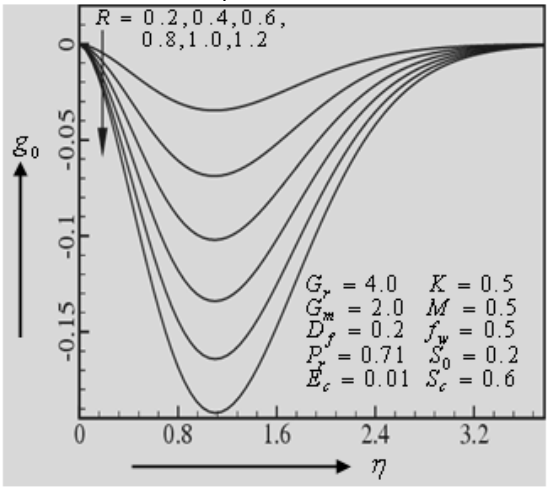

Figure 13: Secondary velocity profiles for different value *R*

In Figures 13-16 the variations of the secondary velocity for different values of rotation parameter R, Soret number S_o, Dufour number D_f and the Eckert number E_c, are shown respectively. From these figures it is observed that the secondary velocity decreases with the increase of rotation parameter R, Soret number S_o, Dufour number D_f and the Eckert number E_c.

In Figs. 17-19, the variations of the secondary velocity for different values of Prandtl number P_r, Schmidt number S_c and permeability parameter K are shown respectively.

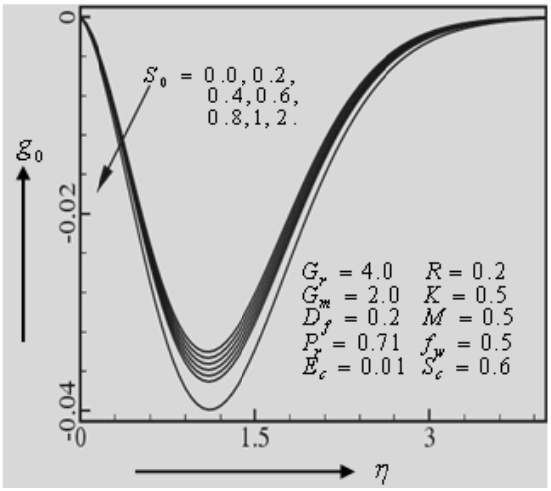

Figure 14: Secondary velocity profiles for different values of S_0

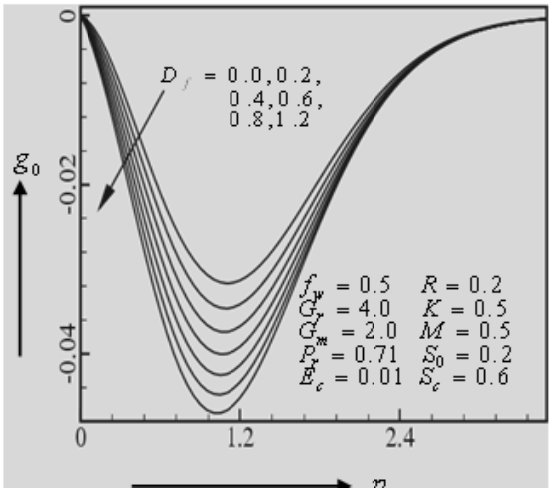

Figure 15: Secondary velocity profiles for different values of D_f

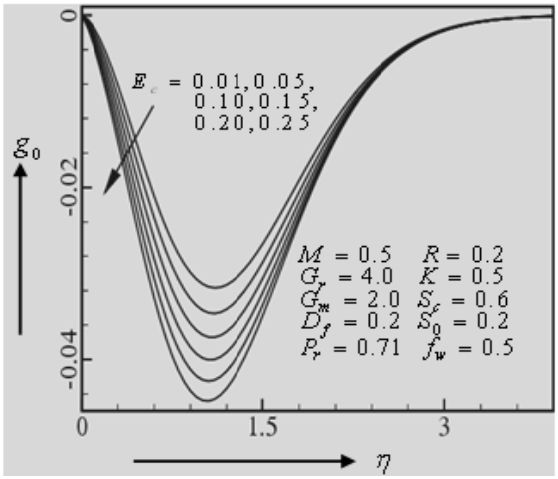

Figure 16: Secondary velocity profiles for different values of E_c

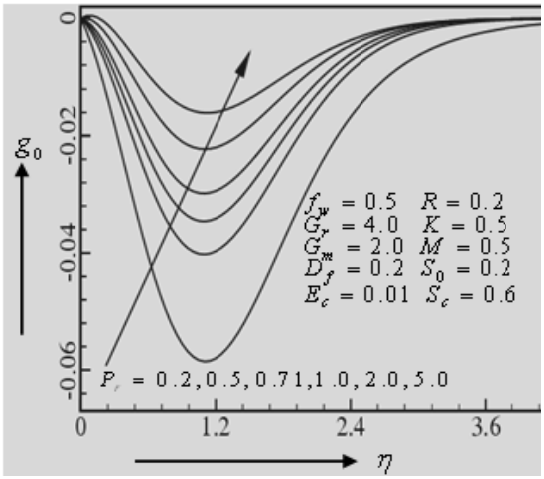

Figure 17: Secondary velocity profiles for different values of P_r

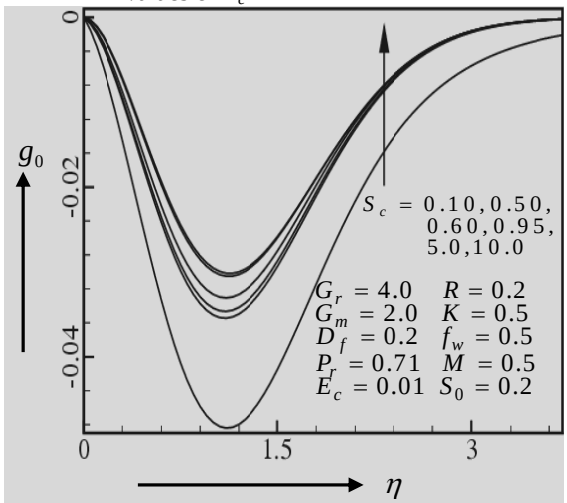

Figure 18: Secondary velocity profiles for different values of S_c

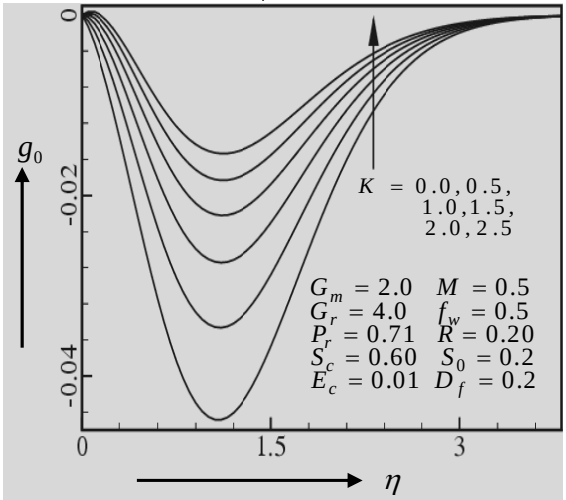

Figure 19: Secondary velocity profiles for different values of K

It is observed from these figures that the large increasing effects are occurred on the secondary velocity with the increase of Prandtl number P_r, Schmidt number S_c and permeability parameter K.The effects of various parameters on non-dimensional temperature are shown in Figs. 20-24. In Fugure 20, the temperature profile for different values of the suction parameter f_w is shown. It is observed from these figures that the temperature increases uniformly with the increase of suction parameter f_w. In Fugure 21, the temperature field for different values of Soret number S_o is shown. It is observed from this figure that the Soret number S_o has a minor decreasing effect on the temperature field. In Fugure 22, the temperature field for different values of Dufour number D_f is shown. It is observed from this figure that the temperature field increases uniformly with the increase of Dufour number D_f.

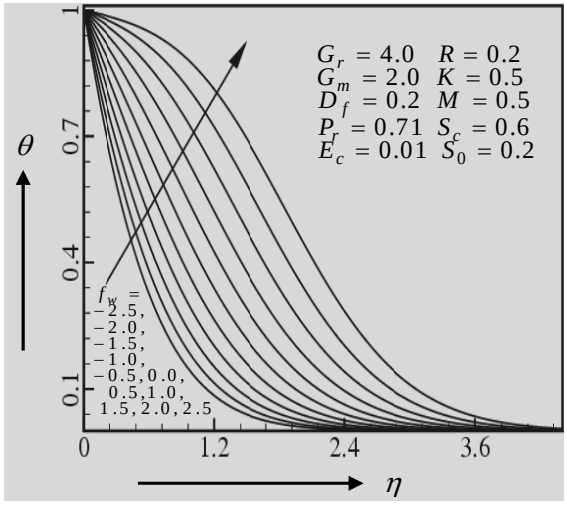

Figure 20: Temperature profiles for different values of f_w

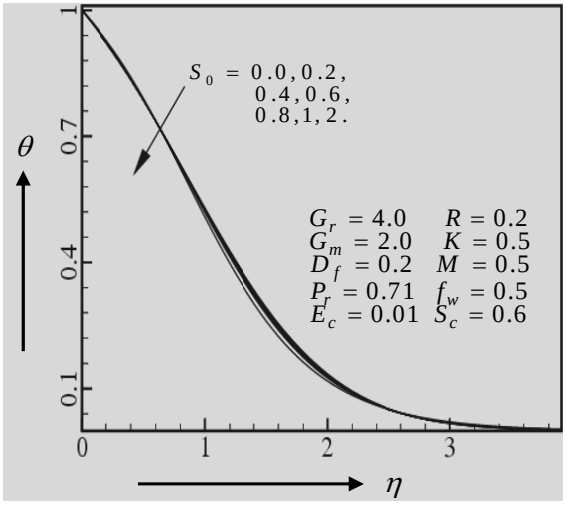

Figure 21: Temperature profiles for different values of S_0

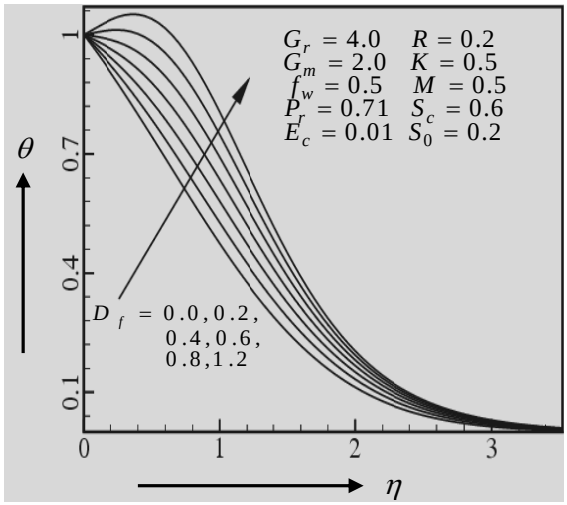

Figure 22: Temperature profiles for different values of D_f

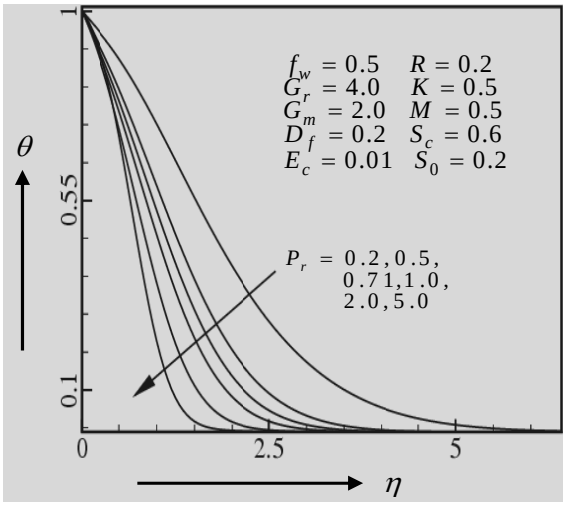

Figure 23: Temperature profiles for different values of P_r

The temperature field is shown in Fugure 23, for different values of Prandtl number P_r. It is observed from Fugure 23 that the Prandtl number P_r has a large decreasing effect on temperature field.

In Fugure 24, the temperature profile for different values of Schmidt number S_c is shown. It is observed from this figure that the Schmidt number S_c has increasing effect on temperature field.

The effects of various parameters on the concentration field are shown in Figs. 25 - 29. In Fugure25, the concentration profile for different values of suction parameter f_w is shown. It is observed from this figure that the concentration uniformly increases as the suction parameter f_w increases.

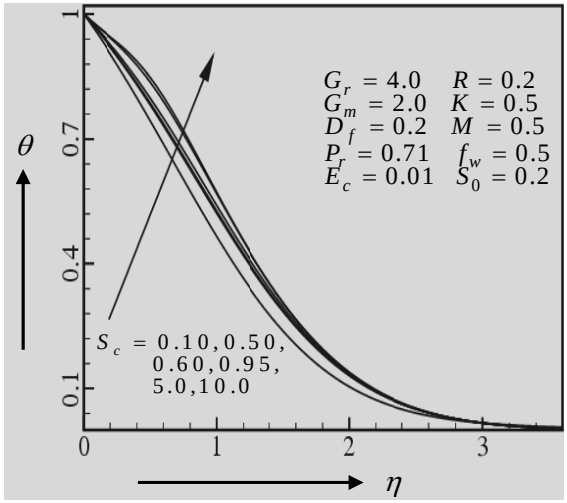

Figure 24: Temperature profiles for different values of S_c

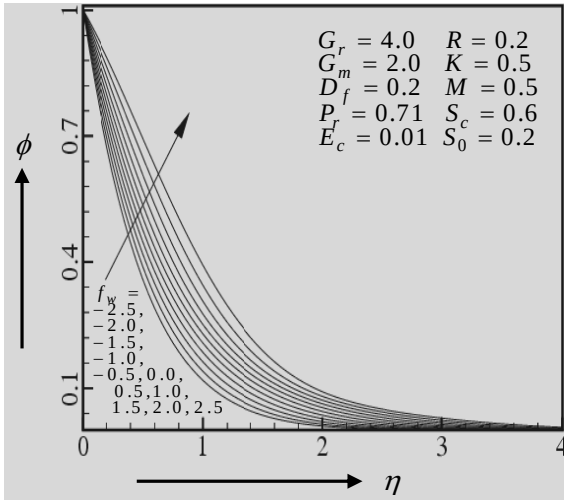

Figure 25: Concentration profiles for different values of f_w

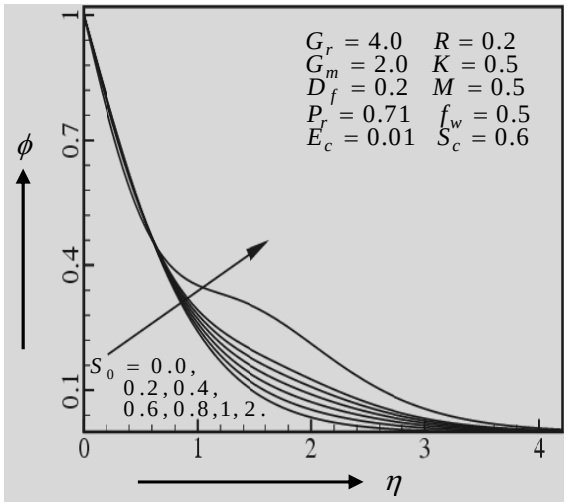

Figure 26: Concentration profiles for different values of S_0

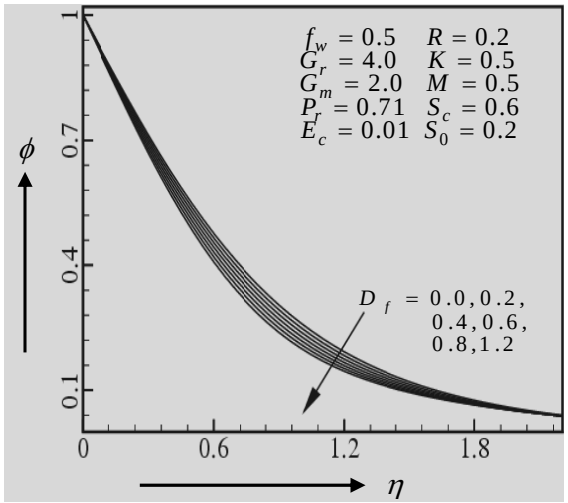

Figure 27: Concentration profiles for different values of D_f

In Fugure 26, the concentration profile for different values of Soret number S_o is shown. It is observed from these figures that the Soret number S_o has decreasing effect on the concentration field. In Figure.27, the concentration profile for different values of Dufour number D_f is shown. It is observed from this figure that the concentration decreases as the Dufour number D_f increases.

In Figures 28-29, the concentration profile for different values of Prandtl number P_r and Schmidt number S_c are shown respectively. It is seen from these figures that the Prandtl number P_r has increasing effect on the

concentration as the Prandtl number P_r increases while the concentration field rapidly decreases with the increase of Schmidt number S_c.

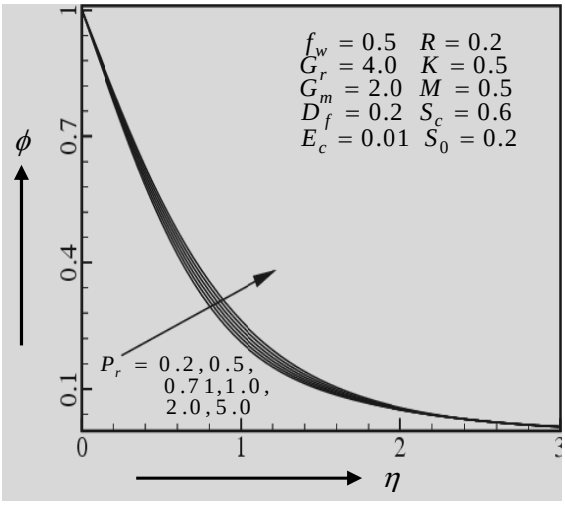

Figure 28: Concentration profiles for different values of P_r

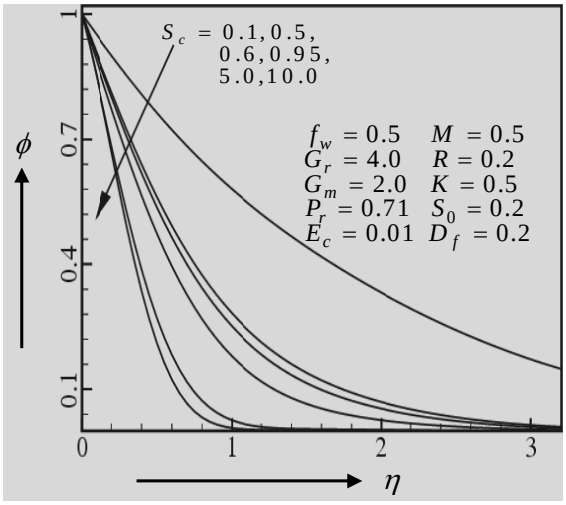

Figure 29: Concentration profiles for different values of S_c

Finally, the effects of various parameters on skin friction coefficients τ_x and τ_z, the Nusselt number N_u and the Sherwood number S_h are shown in Tables 1-5.

Table 1. Numerical values of τ_x, τ_z, N_u and S_h for $G_r = 4.0$, $G_m = 2.0$, $M = 0.5$, $R = 0.2$, $P_0 P_r = 0.71, S_o = 0.2$, $S_c = 0.6$, $D_f = 0.2$, $K = 0.5$ and $E_c = 0.01$

f_w	τ_x	τ_z	N_u	S_h
-2.5	-5.3970229	.0095642	1.6758812	1.8607977
-2.0	-5.1216523	.0052565	1.4084526	1.6964478
-1.5	-4.8538308	.0003204	1.1544840	1.5418072
-1.0	-4.5853473	-.0046324	.9184907	1.3960458
-0.5	-4.3070914	-.0086552	.7053785	1.2573834
00	-4.0104591	-.0105361	.5201109	1.1232665
0.5	-3.6917408	-.0113294	.3663491	.9914265
1.0	-3.3536806	-.0137340	.2458710	.8607047
1.5	-3.0067006	-.0155478	.1577621	.7319121
2.0	-2.6667044	-.0179716	.0983641	.6079297
2.5	-2.3505682	-.0187566	.0618422	.4930417

From Table 1, we observed that the skin friction component τ_x increases while the Nusselt number N_u, the Sherwood number S_h and the skin friction component τ_z decrease with the increase of suction parameter f_w. From Table 2, we observed that the skin friction component τ_x decreases with the increase of magnetic parameter M, while the skin friction component τ_z increases with the increase of magnetic parameter M. It is also observed from this table the skin friction component τ_z decreases while the skin friction component τ_x increases with the increase of magnetic parameter R. We observed from Table 3 that the skin friction components τ_x and τ_z and the Nusselt number N_u decreases with the increase of Soret number S_o, while the Sherwood number

Table 2: Numerical values of τ_x, τ_z, N_u and S_h for $f_w = 0.5$, $G_r = 4.0$, $G_m = 2.0, P_r = 0.71$, $S_o = 0.2$, $S_c = 0.6$, $D_f = 0.2, K = 0.5$ and $E_c = 0.01$

M	R	τ_x	τ_z
0.0	0.2	-3.5022917	-.0220123
0.5	--	-3.6917408	-.0093294
1.0	--	-3.6980711	-.0008342
1.5	--	-3.7164723	.0050039
2.0	--	-3.7435833	.0091054
2.5	--	-3.7770366	.0120398
--	0.2	-3.6917408	-.0093294
--	0.4	-3.6860095	-.0179782
--	0.6	-3.6766617	-.0252933
--	0.8	-3.6639933	-.0306751
--	1.0	-3.6483983	-.0336014
--	1.2	-3.6303484	-.0336476

Table 3: Numerical values of τ_x, τ_z, N_u and S_h for $f_w = 0.5$, $G_r = 4.0$, $G_m = 2.0, P_r = 0.71$, $R = 0.2$, $M = 0.5$, $D_f = 0.2, E_c = 0.01$ and $K = 0.5$.

S_o	S_c	τ_x	τ_z	N_u	S_h
0.0	--	-3.6863470	-.0087116	.3686189	.9793709
0.2	--	-3.6917408	-.0093294	.3663491	.9914265
0.4	--	-3.6970671	-.0099420	.3637905	1.0049244
0.6	--	-3.7023847	-.0105583	.3608885	1.0200427
0.8	--	-3.7075551	-.0111624	.3576506	1.0369413
1.0	--	-3.7126155	-.0117608	.3540188	1.0558461
2.0	--	-3.7355230	-.0146655	.3280050	1.1907625
--	0.10	-3.9076176	-.0253921	.4499665	.5033741
--	0.50	-3.7102878	-.0104183	.3754558	.9377720
--	0.60	-3.6917408	-.0093294	.3663491	.9914265
--	0.95	-3.6490389	-.0070213	.3439702	1.1239821
--	5.00	-3.5444672	-.0024614	.3052763	1.3840714
--	10.00	-3.5234570	-.0016634	.3367076	1.4476235

S_h increases with the increase of Soret number S_o. It is also seen from this table that the skin friction components τ_x and τ_z and the Sherwood number S_h increases with the increase of Schmidt number S_c, while the Nusselt number N_u decreases with the increase of Schmidt number S_c.

From Table 4, we observe that the skin friction components τ_x and τ_z, and the Nusselt number N_u decrease with the increase of Dufour number D_f, while the Sherwood number S_h increases with the increase of Dufour number D_f .It is also observed from this table that the skin friction component τ_x and τ_z and the Nusselt number N_u increase with the increase of Prandtl number P_r while the Sherwood number S_h decreases with the increase of Prandtl number P_r.

From Table 5, we observe that the skin friction component τ_z increases while the skin friction component τ_x decreases with the increase of permeability parameter K. It is also observed from this table that the skin friction

components τ_x and τ_z decrease while the Sherwood number S_h increases with the increase of Eckert number E_c.

Table 4: Numerical values of τ_x, τ_z, N_u and S_h for $f_w = 0.5$, $G_m = 2.0$, $G_r = 4.0$, $K = 0.5$, $R = 0.2$, $M = 0.5$, $S_0 = 0.2$, $E_c = 0.01$ and $S_c = 0.6$.

D_f	P_r	τ_x	τ_z	N_u	S_h
0.0	--	-3.6099163	-.0049333	.4575134	.9688530
0.2	--	-3.6917408	-.0093294	.3663491	.9914265
0.4	--	-3.7758098	-.0136408	.2693714	1.0144665
0.6	--	-3.8622569	-.0178842	.1662347	1.0380500
0.8	--	-3.9510433	-.0220521	.0566285	1.0622193
1.0	--	-4.0423218	-.0261582	-.0598571	1.0870546
1.2	--	-4.1362128	-.0302091	-.1836539	1.1126291
--	0.2	-4.0427357	-.0372245	.2040620	1.0529437
--	0.5	-3.7811806	-.0160653	.3275896	1.0068981
--	0.71	-3.6917408	-.0093294	.3663491	.9914265
--	1.0	-3.6124076	-.0035178	.3938730	.9787620
--	2.0	-3.4827098	.0058550	.3973896	.9651949
--	5.0	-3.3913691	.0134775	.3994546	.9543460

Table 5: Numerical values of τ_x, τ_z, N_u and S_h for $f_w = 0.5$, $G_r = 4.0$, $G_m = 2.0$, $P_r = 0.71$, $R = 0.2$, $M = 0.5$, $S_0 = 0.2$, $D_f = 0.2$ and $S_c = 0.6$.

K	E_c	τ_x	τ_z
0.0	--	-3.6831492	-.0220644
0.5	--	-3.6917408	-.0093294
1.0	--	-3.6975916	-.0008105
1.5	--	-3.7157276	.0050371
2.0	--	-3.7426961	.0091411
2.5	--	-3.7760778	.0120748
--	0.01	-3.6917408	-00932937
--	0.05	-3.7218309	-01053025
--	0.10	-3.7612752	-01209855
--	0.15	-.38029588	-01374844
--	0.2	-3.8471337	-01548839
--	0.25	-3.8940949	-017328202

5. Conclusions

From the result the following conclusions can be drawn:

1. The primary velocity increases with the increase of suction parameter f_w, for both $f_w > 0$ and $f_w < 0$, indicating the usual fact that suction stabilizes the boundary layer growth. While the secondary velocity field decreases with the increase of suction parameter f_w, for both $f_w > 0$ and $f_w < 0$.
2. The primary velocity for different values of magnetic parameter M and has a decreasing effect with increase of M. The magnetic field can therefore be used to control the flow characteristics. The Prandtl number P_r has increasing effect on the concentration as the Prandtl number P_r increases while the concentration field rapidly decreases with the increase of Schmidt number S_c.

3. For larger values of P_r $(P_r = 0.5)$ and S_c the velocities are found to decrease monotonically and hence there appears a thin boundary layer indicating the decrease of the free convection.
4. The temperature and concentration increases uniformly with the increase of suction parameter f_w. The Soret number S_o has decreasing effect on the concentration field. The Soret number S_o has decreasing effect on the concentration field.

References

Anghel, M., Takhar, H.S. and Pop, I. (2000): Dufour and Sorret effects on free convection boundary-layer flow over a vertical surface embedded in a porous medium. Studia Univ. Babes-Bolyai. Mathematica. XLV, pp.11-21.

Alam, M. S. and Rahman, M. M. (2006): Dufour and Soret effects on mixed convection flow past a vertical porous flat plate with variable suction, Nonlinear analysis: Modeling and Control, Vol. 11, No. 1, 1-10.

Debnath, L. (1975): Inertial oscillations and hydromagnetic multiple boundary layers in a rotating fluid, Journal of Applied Mathematics and Mechanics (Zeitschrift für Angewandte Mathematik und Mechanik, ZAMM), 55, 141.

Debnath, L., Roy, S. C. and Chatterjee, A. K. (1979): Effects of hall current on unsteady hydro-magnetic flow past a porous plate in a rotating fluid system, Journal of Applied Mathematics and Mechanics (Zeitschrift für Angewandte Mathematik und Mechanik, ZAMM), **59:** 469.

Eckert, E. R. G, and Drake, R. M. (1972). Analysis of Heat and Mass Transfer, McGraw- Hill Book Co., New York.

Hossain, M. A.(1990): MHD forced and free convection flow with joule heating, International Center for Theoretical Physics (ICTP), Italy, Internal Print no IC/90/265.

Kafoussias, N. G. and Williams, E. M. (1995): Thermal-diffusion and diffusion-thermo effects on mixed free-forced convective and mass transfer boundary layer flow with temperature dependent viscosity, International Journal of Engineering Science, vol. 33, no. 9, pp.1369-1384. http://dx.doi.org/10.1016/0020-7225(94)00132-4

Pai, S. I. (1962): Magnetogasdynamics and Plasma dynamics, Springier Verlag, New York.

Postelnicu, A. (2004): Influence of a magnetic field on heat and mass transfer by natural convection from vertical surfaces in porous media considering Soret and Dufour effects, Internatonal Journal of Heat and Mass Transfer, vol. 47, no.6-7, pp.1467-1472. http://dx.doi.org/10.1016/j.ijheatmasstransfer.2003.09.017

Raptis, A. A. and Perdikis, C.P. (1982): Effects of mass transfer and free-convection currents on the flow past an infinite porous plate in a rotating fluid, Astrophysics and Space Science, vol. 84, no. 2, pp.457-461. http://dx.doi.org/10.1007/BF00651324

Sattar, M. A. (1993): Free and forced convection boundary layer flow through a porous medium with large suction, International Journal of Energy Research, 17, pp.1-7, http://dx.doi.org/10.1002/er.4440170102.